

JGR Atmospheres

RESEARCH ARTICLE

10.1029/2021JD035467

Key Points:

- Occurrence of long-lived Rossby Wave Packets shows large interannual variability in southern hemisphere summer
- Intense negative Southern Annular Mode phases favor the occurrence of long-lived Rossby Wave Packets
- Long-lived Rossby Wave Packets last longer in strong negative SAM events compared to its positive phase

Supporting Information:

Supporting Information may be found in the online version of this article.

Correspondence to:

I. Pérez,
iperez@fisica.edu.uy

Citation:

Pérez, I., Barreiro, M., & Masoller, C. (2021). ENSO and SAM influence on the generation of long episodes of Rossby Wave Packets during southern hemisphere summer. *Journal of Geophysical Research: Atmospheres*, 126, e2021JD035467. <https://doi.org/10.1029/2021JD035467>

Received 28 JUN 2021
Accepted 15 NOV 2021

ENSO and SAM Influence on the Generation of Long Episodes of Rossby Wave Packets During Southern Hemisphere Summer

Iago Pérez¹ , Marcelo Barreiro¹ , and Cristina Masoller² 

¹Departamento de Ciencias de la atmósfera, Facultad de Ciencias, Universidad de la República, Montevideo, Uruguay,

²Physics department-Nonlinear, Universitat Politècnica de Catalunya, Terrasa, Barcelona, Spain

Abstract This study assesses the impact of low-frequency climate modes on Rossby Wave Packets (RWPs) during southern hemisphere summer. In particular, we focus on long-lived RWPs (lifespan above 8 days) and determine how El Niño-Southern Oscillation (ENSO) and the Southern Annular Mode (SAM) influence their statistics, that is, their duration, frequency of occurrence, and activity areas. We used daily mean meridional winds at 300 hPa from December to March between 1979 and 2020 from the ERA5 and NCEP-DOE 2 reanalyses. We found that long-lived wave packets, which are a small percentage of the total number of wave packets, show large interannual variability; there are years in which these types of waves do not occur and years that present up to 9 wave packets. This suggests that large-scale circulation conditions set up by low-frequency climate modes can modulate their occurrence. Classifying years according to SAM phases reveals that the occurrence of long-lived RWPs is highest (lowest) during intense negative (positive) SAM events. ENSO influence, on the other hand, was found to be weak and not robust. Analysis of large scale circulation conditions shows that during negative SAM phases the jet shifts northward, strengthens in the Indian sector, and extends further into the Pacific basin, so that it acts as a better waveguide favoring the propagation of long-lived RWPs. Conversely, during positive phases of SAM, the jet shifts southward and an anticyclonic center develops to the southwest of Australia blocking the jet and the progression of the wave packets.

1. Introduction

Atmospheric circulation in mid-latitudes is dominated by the upper level jet and associated storm track. It is well known that atmospheric predictability on time scales longer than the synoptic is limited due to the chaotic nature of the atmosphere, while on seasonal timescales predictability is strongly dependent on tropical surface ocean conditions. On intermediate, subseasonal scales, predictability relies on persistent structures such as atmospheric blockings or Rossby Wave Packets (RWPs). RWPs are packets of upper-level atmospheric waves that are able to travel coherently for several days by downstream development (Tu-Cheng Yeh, 1949; Chang & Yu, 1999; Chang, 2000) and transport large quantities of energy. These packets are constantly being created and destroyed in mid-latitudes and most of them survive only for a few days, but under certain conditions, these packets can be stable and propagate for several days or even weeks before disappearing (Grazzini & Vitart, 2015).

RWPs represent high-amplitude meanderings of the jet stream and thus are related to storm track variability (Souders et al., 2014a). Moreover, they have been recognized as precursors of extreme weather such as heat waves or extreme rainfall events, (Chang, 2005; O'Brien & Reeder, 2017; Wirth et al., 2018), as well as extratropical cyclone development, (Chang et al., 2005; Sagarra & Barreiro, 2020). Additionally, it has been shown that RWPs affect the weather forecast in the areas they cross, increasing the uncertainty on short and middle range forecasting (Zheng et al., 2013; Souders et al., 2014b). Increasing our knowledge about processes that control RWPs is thus crucial to understand the mechanisms that affect weather and climate in mid-latitudes and provides the possibility of extending the forecast beyond synoptic timescales (Grazzini & Vitart, 2015).

As mentioned earlier, under certain conditions RWPs can maintain their coherence longer than usual and are able to survive for weeks in the atmosphere. The lifespan, extension and propagation of RWPs are highly dependent on the potential vorticity gradient and the distribution of diabatic heating sources (Grazzini & Vitart, 2015). Potential vorticity (PV) gradients control the strength and position of the waveguide where RWPs propagate (Hoskins & Ambrizzi, 1993), such that a very intense and narrow gradient of PV favors the development of coherent RWPs that will last longer in the atmosphere before they disappear, (Chang & Yu, 1999; Souders et al., 2014b; Manola

et al., 2013, Wirth, 2020). On the other hand, weaker gradients tend to stop or attenuate wave propagation (Grazzini & Vitart, 2015). The role of jets as waveguides that favor the propagation of packets in the zonal direction has been studied extensively in the Northern Hemisphere (e.g., Hoskins & Ambrizzi, 1993; Branstator, 2002; Xu et al., 2019; Teng & Branstator, 2019; Xu et al., 2021).

RWPs are more easily detected in the southern hemisphere due to the absence of baroclinically unfavorable continental areas (Grazzini & Vitart, 2015). Moreover, during austral summertime, the storm track is almost zonally symmetric at 50°S and the jet presents a wind speed maximum in the Atlantic-Indian sector that acts as a waveguide (Hoskins & Ambrizzi, 1993; Chang, 1999). In the southern hemisphere (SH) there are, however, few studies on RWPs and these are mainly focused on climatological characteristics and statistics. For example, Chang, (1999) found that wave packets tend to propagate along the mid-latitude jets and that their zonal group velocity in the SH summer is about 20–25 m/s. In Chang, (2000) it was shown that most wave packets propagate when dominated by downstream development, and that a surface cyclone developed in nearly all cases to the east of the upper-level troughs associated with the wave packets. Additionally, Souders et al., (2014a) showed that RWPs activity in the SH does not have a strong seasonal cycle and that the packets detected are faster and more coherent than in the northern hemisphere. They also found a positive trend in the annual mean activity of RWPs that they hypothesize may be related to an improvement of the quality of the reanalysis (consistent with Barreiro et al., 2014) or to the observed trend in the Southern Annular Mode (SAM) during summer.

Barreiro, (2017) studied the interannual variability of wave activity during austral summertime in the southeast Pacific-Atlantic sector and found that the leading pattern of variability in this region is correlated with El Niño Southern Oscillation (ENSO), such that there is an increase in transient wave energy in the Pacific during El Niño years. However, this study did not address the characteristics of RWPs. Sagarra and Barreiro, (2020) performed a climatological study of RWPs during the austral summer in the SH and found a mean of 32 packets per season, 90% of the trajectories have a lifespan of 3–8 days and 80% of the waves propagated between 30 and 170° degrees of longitude. No main area of dissipation/formation on seasonal or monthly timescales was detected and the study did not find a relation between the interannual count of RWPs and ENSO, but suggested a possible relationship with SAM.

The interannual variability of RWPs and the influence of global climate modes on RWPs have not been yet addressed in detail. The goal of the present study is to fill this gap by studying the impact of ENSO and SAM on the characteristics of RWPs during austral summer. It is well known that these climate modes alter the large-scale mid latitude flow and therefore, the waveguide where the RWPs propagate. We will focus on long-lived RWPs, (hereafter LLRWPs), which are those that live longer than 8 days (Grazzini & Lucarini, 2010), having in mind that understanding how climate modes modulate the occurrence and propagation characteristics of RWPs, as well as how they modify the areas where these long-lived packets are detected, may contribute to the improvement of extended range forecasting (between 10 and 30 days) of extreme weather events. The robustness of the results is addressed considering two independent reanalyses.

This paper is organized as follows. Section 2 describes the data, the tracking algorithm, and the analysis applied in this study. Section 3 describes the climatology and interannual variability of RWPs. Section 4 focuses on the impact of ENSO and SAM on LLRWPs and Section 5 addresses the large-scale conditions and mechanisms that favor LLRWPs. Lastly, Chapter 6 provides a summary of the results.

2. Data and Methods

2.1. Data

To track RWPs, we use daily mean meridional winds (m/s) at 300 hPa as done previously by several authors (e.g., Chang & Yu, 1999; Sagarra & Barreiro, 2020). The data used in this study comes from the ERA5 reanalysis (Hans et al., 2020) with an horizontal resolution of 0.25° x 0.25° and from the NCEP-DOE Reanalysis 2 (NOAA/OAR/ESRL) (Kanamitsu et al., 2002), with a horizontal resolution of 2.5° x 2.5°. The period of study chosen is the austral summer here considered as December, January, February, and March (DJFM) from 1 December of 1979 to 31 March of 2020, thus retaining data corresponding to 41 summer seasons. We included March in the analysis to increase the sample size because long-lived RWPs represent close to 10% of the total packets registered. Barreiro, (2017) and Sagarra & Barreiro, (2020) concluded that the characteristics of RWPs detected in March are very similar to those detected in the traditional DJF months of the summer season.

RWPs are generally composed of a series of troughs and ridges confined to a certain zonal band, and thus to characterize them we compute the envelope that encloses the wave packet. As a result, each RWP is characterized by an envelope whose amplitude has highest values at the center and decreases to the east and west. To compute the envelope using the meridional winds at 300 hPa, we proceed in three steps: (i) calculation of the anomalies by removing the daily climatology, (ii) the subtraction of the seasonal mean in order to remove the interannual variability, (iii) calculation of the amplitude of the wave packet envelope (m/s) using the methodology of Zimin et al., (2003). We retained wave numbers between 4 and 11, which are representative of the atmospheric transients in the SH (Trenberth, 1981). For the methodology of Zimin et al., (2003) to work well, the propagation of RWPs has to be in the zonal direction (e.g., Zimin et al. (2006), which is the case for the SH summer as shown by Chang, (1999). This latter study also showed that the jet and maximum variance in meridional wind anomalies are in a band centered at 50° S, and therefore in our study, we averaged latitudinally data in the band 40°S–65°S.

To characterize the interannual occurrence of the global climate modes, we considered for ENSO the Oscillation Niño Index (ONI) and for SAM the Antarctic Oscillation index (AAO). Both data sets are available from the NOAA website. Of the 41 years considered, 14 years are classified as El Niño, 13 years as La Niña, and 14 years as Neutral years. In the case of SAM, we also classified years as positive, negative, and neutral. To do so, first we subtracted the linear trend of the SAM index for the 41 seasons. Next, we applied the following criteria: if the absolute value of the detrended seasonal SAM index in a year t surpasses the threshold of 0.35σ (σ is the standard deviation of the detrended SAM index) that year is classified as SAM positive (SAM negative) if the value is positive (negative). Conversely, if the seasonal SAM index is below this threshold, it is considered a neutral year. The reason to choose this threshold is to retain a similar number of positive SAM and negative SAM years. As a result, 9 years correspond to negative SAM, 11 years to positive SAM and 21 years to neutral SAM.

We also used geopotential height (Z_{300}) and zonal winds at 300 hPa (u_{300}), as well as sea surface temperature (SST) from the ERA5 reanalysis to study the upper level circulation anomalies and surface ocean conditions, respectively, associated with the interannual variability in the occurrence of RWPs. Also, to characterize changes in the position and intensity of the waveguide, we calculated the meridional gradient of the absolute vorticity (mAVg, also at 300hPa), which is commonly used as an approximation of the isentropic gradients of potential vorticity (Wirth et al., 2018).

2.2. Methodology

2.2.1. Tracking Algorithm and RWPs Classification

Before applying the algorithm to track RWPs, we set a minimum threshold for the amplitude of the envelope to avoid tracking noise. The value of this threshold should be selected carefully, in order to be able to distinguish one packet from another (Souders et al., 2014b). If the threshold is too low, the algorithm will track noisy fluctuations, while if it is too large, the algorithm will miss some RWPs. In the case of the ERA5 data set, we decided to use 19 m/s as a minimum threshold in the calibration stage. For the case of the NCEP-DOE 2 data set, Grazzini & Vitart, (2015) considered a threshold value of 16 m/s, Souders et al., (2014b) 14 m/s, and Sagarra & Barreiro, (2020) 15 m/s. Therefore, in our study, we decided to apply a threshold of 15 m/s for the NCEP-DOE 2 data set. Nonetheless, in order to study the sensitivity of the results, we also considered a 2 m/s higher and lower threshold for each reanalysis. The choice of a higher threshold for ERA5 is based on the fact that this reanalysis showed larger mean values of the amplitude of the envelope, thus representing a jet stream characterized by stronger meandering probably due to the higher resolution of the data set.

The algorithm tracks the amplitude of the envelope above the chosen threshold allowing to follow a coherent wave packet in its trajectory and consists of the following steps:

1. Detection of the highest value of the amplitude in the longitudinal axis (p_n) in the first day of the data matrix.
2. Search for the position of the maximum amplitude eastwards in the next day (p_{n+1}).
3. If the points p_n and p_{n+1} are between $[p_n + 15^\circ$ to $p_n + 45^\circ]$, p_n and p_{n+1} are registered as part of the same trajectory and we repeat steps 2 and 3 for the following days. The distance is chosen so that the wave packet travels at a speed between 15 and 45° per day as found in (Sagarra and Barreiro 2020).
4. When we find a maximum p_m that it is not within the range specified in step 3 or when we reach the limit of the data matrix, the trajectory is saved and we resume the tracking from the last day we detected the start of a trajectory.

5. After analyzing all longitudes for the day, we proceed to the next one and repeat steps 1–4 until we analyzed the whole data matrix.
6. Having finished the analysis of the data matrix, we check for trajectories that may have been truncated and apply proximity criteria as follows. If two trajectories are closer than 1000 km and their difference in slope is less than 20°/day they are joined. Additionally, for slow trajectories that were separated by 1–2 days, but the mean speed between the end of a trajectory and the start of the next one is less than 15°/day, they are considered as a single trajectory if the mean speed between points L–1 or L (being L the last point of the first trajectory) to I or I+1, (being I the initial point of the second trajectory) is 15°/day or above and the mean envelope between the two trajectories surpasses the minimum threshold.
7. Finally, we filtered out trajectories with a lifespan below three days because they are not relevant to this study.

After running the algorithm, we performed a statistical analysis of the RWP detected. The following measures were considered: (i) mean propagation speed (m/s) taking into consideration that 1°/day is approximately 0.82 m/s in the latitudinal region analyzed (40–65°S), (ii) duration (days during which a trajectory can be tracked until it disappears), (iii) length of the trajectory (difference between the starting and ending point of the trajectory) in degrees and (iv) activity areas. Then, we studied the interannual variability of LLRWPs and the impact of global climate modes.

RWPs are classified into three categories based on their lifespan: short-lived RWPs if their lifespan ranges between 3 and 6 days, medium-lived RWPs when their lifetime ranges between 7 and 8 days and LLRWPs when they last more than 8 days. Although we focused on long-lived packets, RWPs of different lifespans were registered to study whether their frequency of occurrence is correlated. As mentioned above, to study the robustness of the results, we considered several thresholds in the tracking algorithm for ERA5 and NCEP-DOE 2 data sets. For ERA5, we used the thresholds 17, 19, and 21 m/s, and for NCEP-DOE 2 the thresholds 13, 15, and 17 m/s. The Kruskal Wallis test was used to determine whether the results obtained classifying the years according to the different ENSO/SAM phases are statistically different from each other, highlighting results that reach a 10% significance level.

To study the areas of activity of LLRWPs, we considered the following six regions: 0–60°E, 61–120°E, 121–180°E, 181–240°E, 241–300°E, and 301–359°E. We calculated the frequency (%) of RWPs propagating in these regions, for all years and separating according to ENSO and SAM phases.

2.2.2. Analysis of Large-Scale Conditions

The identification of atmospheric and oceanic conditions that favor the formation and propagation of LLRWPs was assessed using regression and composite analyses. We regressed u_{300} , $mAVg$, Z_{300} and SST anomalies onto the time series of interannual occurrence of LLRWPs, assessing the statistical significance of the results obtained using a Student's t-test at 10% significance level. The regression field allows distinguishing ocean and atmospheric circulation anomalies associated with the global climate modes of interest (ENSO and SAM).

To complement the regression analysis, we selected the years with the highest and lowest frequency of occurrence of LLRWPs tracked in the ERA5 data set (for a threshold of medium intensity), and constructed composite maps of seasonal mean u_{300} and $mAVg$ for these years. Years of maximum (minimum) LLRWPs occurrence are considered as those above (below) one standard deviation. Additionally, we subtracted seasonal mean wind (u , v) at 300 hPa during years of maximum LLRWPs detection against years of minimum detection to determine the regions that are statistically different using a Student's t-test. This also provides insight into the physical mechanisms that favor/disfavor LLRWPs formation and propagation.

The results shown below are mainly based on ERA5, including a comparison with NCEP-DOE 2 when it adds relevant information.

As mentioned in the Introduction, jets can act as waveguides. Thus, to test whether years with maximum occurrence of LLRWPs are related to changes in the jet, we calculated the wave coherence index (WCI). Chang & Yu, (1999) & Chang, (1999) showed that the maximum values of the WCI identify the regions where the upper level jet acts as a waveguide, and other studies have used the WCI to study the interannual variability of waveguides (e.g., Seager et al., 2010). Thus, we expect LLRWPs to be favored during years when the WCI is maximum and zonally continuous.

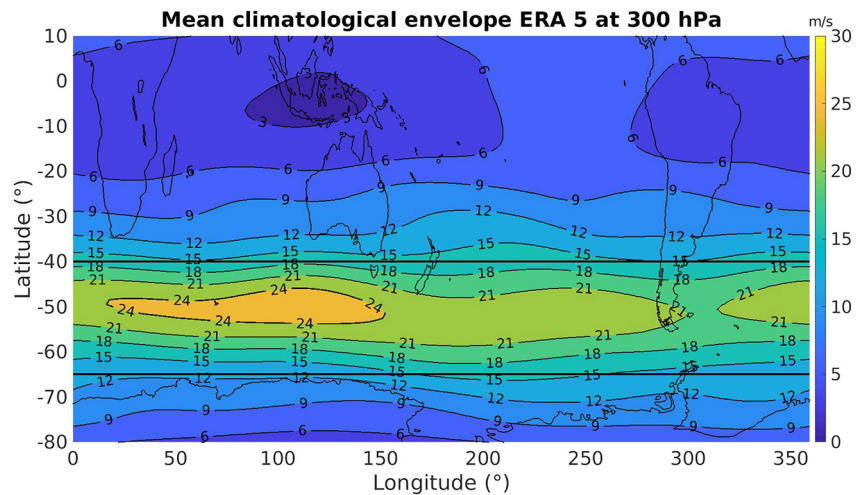


Figure 1. Mean climatological amplitude (m/s) during DJFM. Solid black lines show the area of study.

To study the interannual variability, we first calculated the WCI for each year using the daily mean meridional wind at 300 hPa (from ERA5) and the methodology described in Chang, (1999). Then, we performed a Principal Component Analysis (PCA) of the yearly WCI in order to identify the main modes and relate them to the occurrence of LLRWPs, ENSO and SAM. The PCA analysis was done in the latitudinal band 30°S–70°S and the data was weighted by $\cos(\text{latitude})^{1/2}$.

3. Mean and Interannual Variability of RWPs

Figure 1 shows the climatological amplitude of the envelope in the SH summer for ERA5. The highest values of the amplitude are located in the latitudinal band between 40 and 60°S as expected, and from 25 to 150°E (Figure 1). There is a minimum located around the southern tip of South America consistent with the results of Souders et al., (2014a) (in their case on an annual timescale). The spatial structure is similar on individual months (not shown). As a result, RWPs tracked using restrictive thresholds could be abruptly interrupted close to South America and may cause a reduction of LLRWPs in the areas between 280 and 330°E.

The total number of RWPs detected in this analysis using ERA5 is 1256 packets, being 141 the number of packets that lasted more than 8 days, corresponding to about a total of 30 (3) RWPs (LLRWPs) per season. Figure 2 presents a summary of statistics of RWPs properties. Figure 2(a) shows an exponential decrease in the duration of the wave packets such that about 77% do not reach 7 days and about 1.1% of the trajectories have a lifespan of 14 days or above during the season. In addition, Figure 2(b) shows that 78% of the trajectories travel between 30° and 170° in the longitudinal direction and only about 2.45% are able to complete a full latitudinal circle. The mean distance travelled by a packet is 126°, the median is 96°, and the inter-quartile range is 101°. In the case of their lifespan, they show a mean duration of 5.3 days, a median of 4 days, and an interquartile range of approximately 6 days. Figure 2(c) shows the RWPs speed distribution with a mean speed of 20.7 m/s and a standard deviation of 5 m/s.

In the case of the NCEP-DOE2 data set, we detected 1225 RWPs, 101 being LLRWPs. About 70% of the trajectories do not reach 7 days, and barely 2% of the trajectories detected surpass 14 days. The mean distance travelled by RWPs is 128°, with a median of 84°, and an interquartile range of 85°. RWPs duration display a mean of 5 days, a median of 4 days, and an interquartile range of 3 days. Lastly, the mean speed is 20.5 m/s with a standard deviation of 4.3 m/s. Thus, the results obtained in NCEP-DOE 2 are very similar to those obtained using ERA5.

In comparison, Sagarra & Barreiro (2020) found that the mean speed of the packets is 20 m/s with a standard deviation of 6.6 m/s and a mean lifespan of almost 6 days per packet. Overall, 80% of the packets lasted between 3 and 7 days and around 1% surpasses the 14 days threshold. They also found that packets trajectory has a mean of 99° of longitude. Overall, the results obtained in this study are similar to those obtained in Sagarra & Barreiro, (2020).

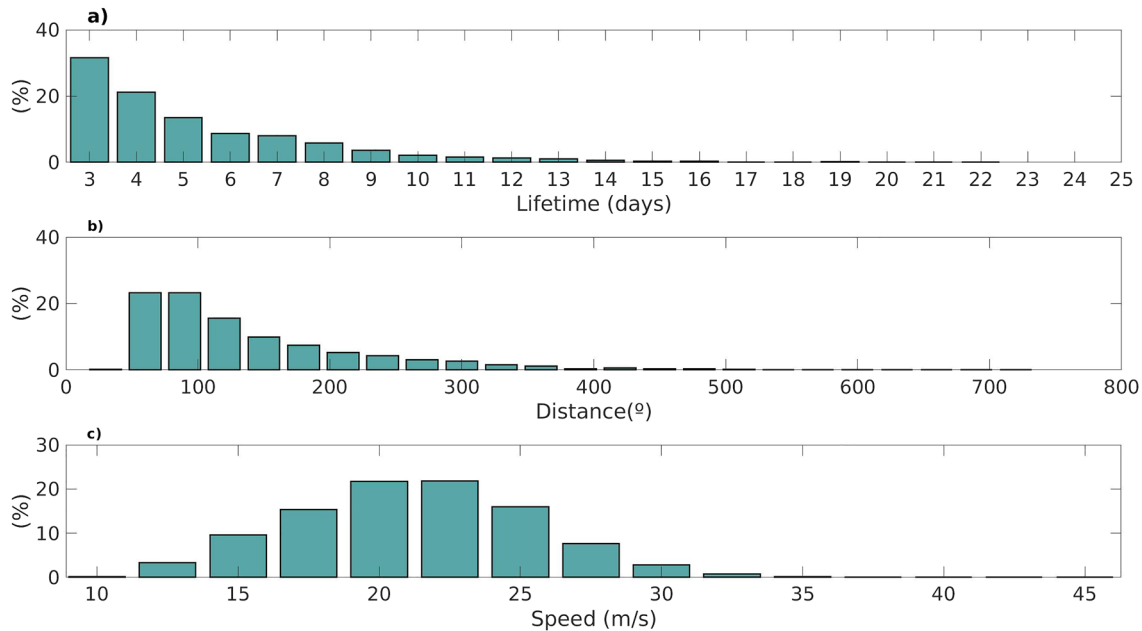


Figure 2. Climatological properties of RWPs tracked between 1979 and 2020 during DJFM using a minimum threshold of 19m/s; (a) lifespan, (b) distance travelled, and (c) the mean speed per packet.

On the other hand, Souders et al., (2014b) found that in the SH, 70% of the RWPs detected lasted less than 8 days, with a mean lifetime of 7.9 days and a mean of 151 degrees of distance travelled. The mean duration and distance travelled found in our study are lower compared to Souders et al., (2014b), which could be, in the case of the NCEP-DOE 2 data set, at least partially explained by the use of a less restrictive threshold in that study (14 m/s).

As shown in Figure 3(a), the frequency of occurrence of the total number of RWPs in ERA5 shows large interannual variability, with values in the range of 20 and 40 packets per year. The dependence on the threshold chosen is not strong as the time series of RWPs detected are highly correlated for different thresholds. While results are very similar for 17 m/s and 19 m/s, there is a reduction in the mean number of packets detected during the whole period for a threshold of 21 m/s. This may be related to the fact that the isoline of 21 m/s shows a break in the south Atlantic in the mean conditions (see Figure. 1).

Looking at subsets of RWPs, it is clear that the overall behavior of the total number of events is dominated by the variability in the occurrence of short-lived waves (Figure 3b). For medium-lived and long-lived waves (Figures. 3c and 3d), the number of events per year is similar: it is relatively small and it increases when using a lower threshold. In addition, long-lived wave packets show large interannual variability existing years without these type of waves and others that present up to 9 packets. This suggests that large-scale circulation conditions set up by low-frequency climate modes can modulate their occurrence. Figure S1 shows the time series of occurrence of LLRWPs identifying the corresponding ENSO and SAM phases during each year.

Furthermore, it is also worth mentioning that there is a negative correlation between the occurrence of short-lived and long-lived waves with $r = -0.32$ for a threshold of 19 m/s, so that the detection of several long-lived waves also results in less short-lived waves during that particular year. This correlation value is statistically significant at 5% level according to Student's t-test.

The wave activity of all RWPs, shown in Figure 4(a), has a maximum at around 61–121° E (Indian ocean) and a minimum between 181 and 240°E (eastern Pacific basin). These results are similar to those found in Souders et al., 2014a. In contrast, the median of wave activity for LLRWPs is uniform across all longitudes, although longitudes to the east of 120°E have years with few packets (Figure 4b). Regarding the influence of ENSO on LLRWPs activity, we did not find any meaningful differences between the activity areas during El Niño or La Niña, (not shown). In the case of SAM, there is also no zonal dependence of the median in wave activity, but

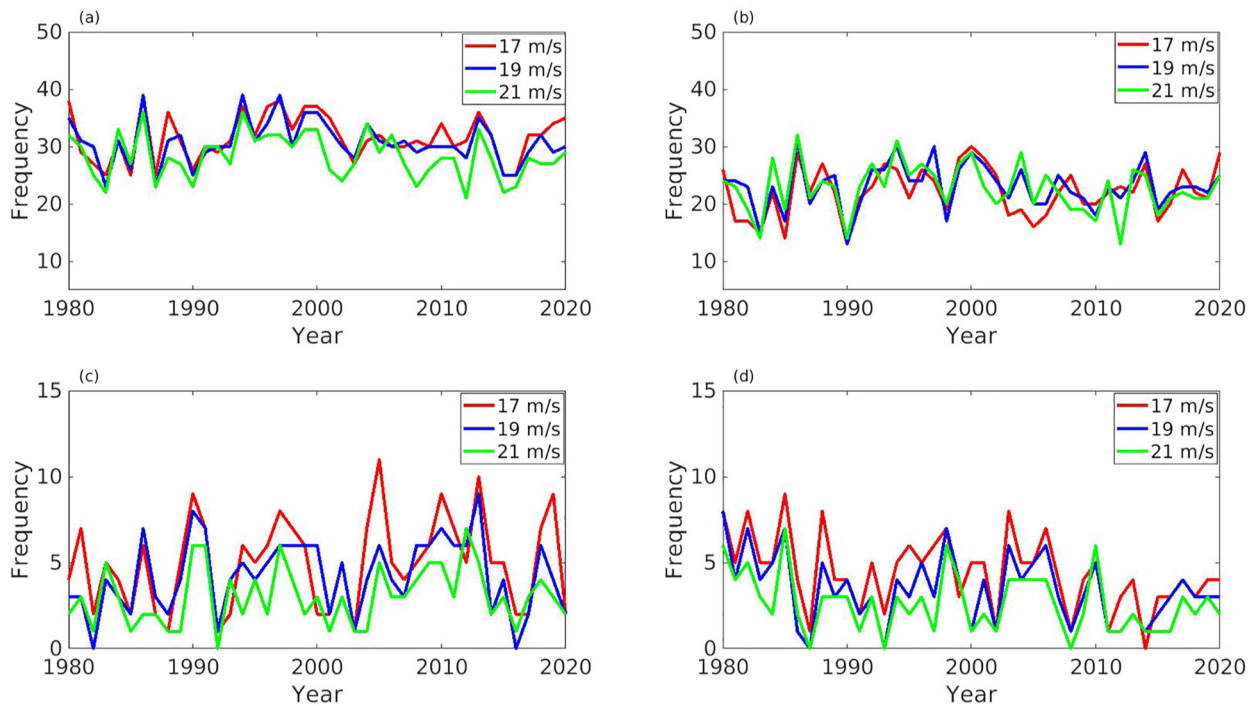


Figure 3. Interannual variability of the total RWP activity (a), short-lived waves (b), medium-lived waves (c), and long-lived waves (d). Red, blue, and green lines indicate the results obtained using thresholds of 17, 19, and 21 m/s, respectively.

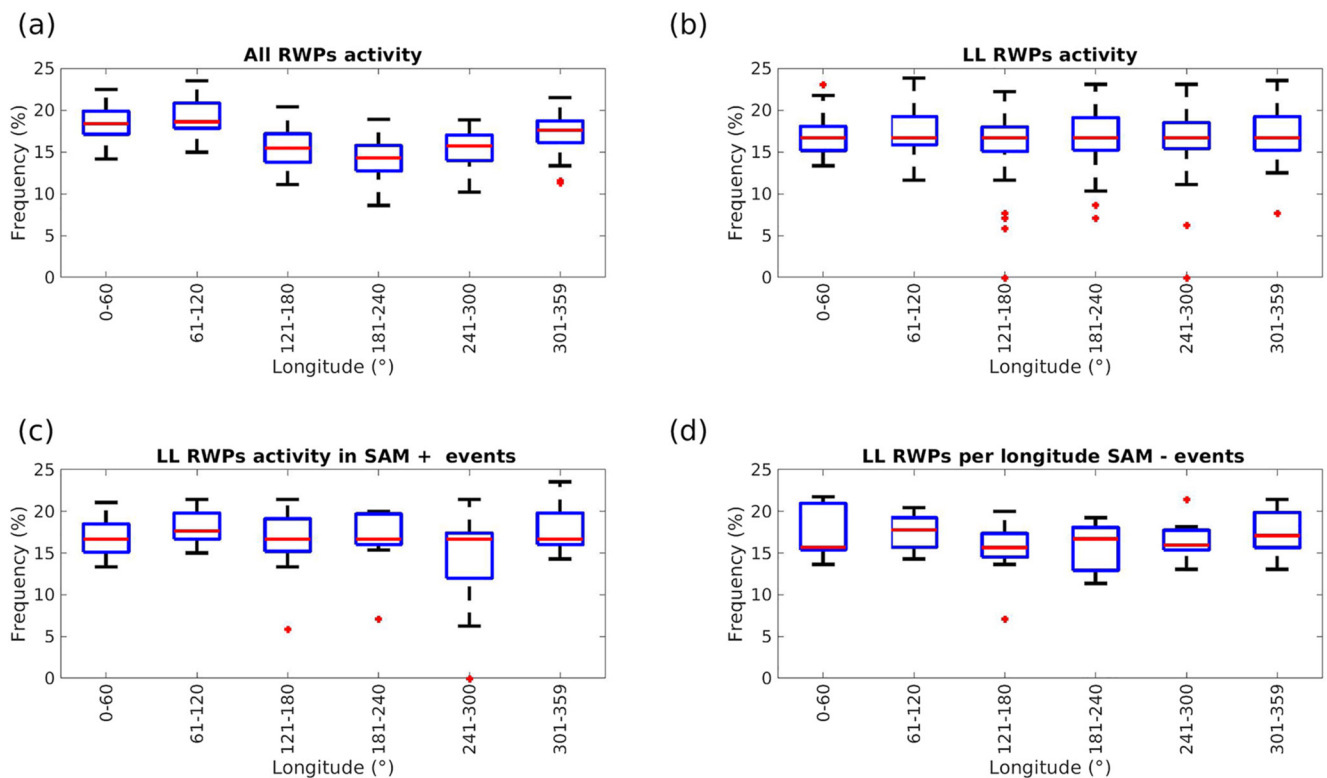


Figure 4. Boxplot of RWP activity in ERA5 for (a) all RWP and (b) for LLRWP. The bottom panel shows the influence of SAM on wave activity of LLRWP: (c) for SAM+ phase and (d) for SAM – phase. Red crosses indicate the presence of outliers.

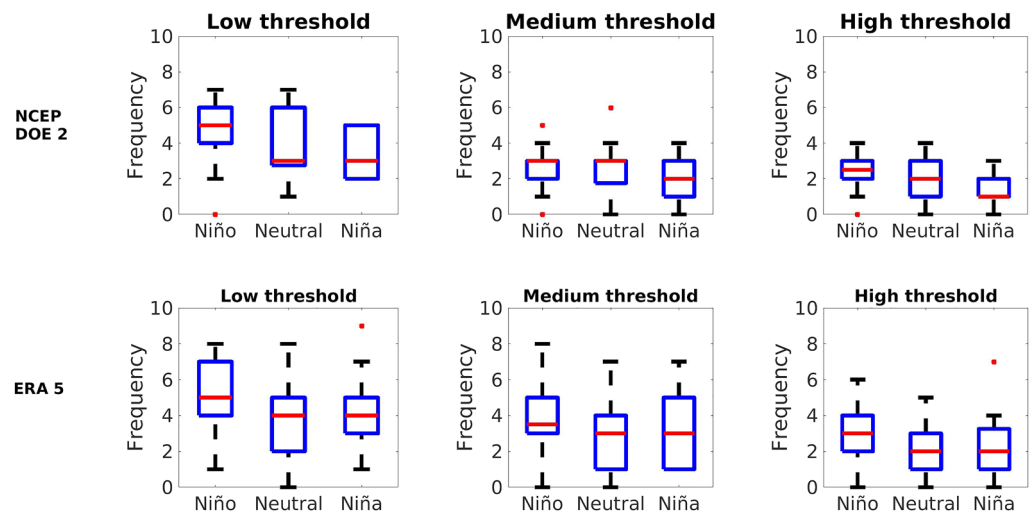


Figure 5. Boxplots of interannual variability of LLRWPs detected during different ENSO phases using NCEP-DOE 2 (upper panels) and ERA5 (lower panel) for different thresholds. Red crosses show outliers and red lines show the median location. The title of each boxplot refers to the threshold applied in the tracking stage. Low threshold is 17 (13 m/s), medium threshold is 19 (15 m/s), and high threshold is 21 (17 m/s) for ERA5 (NCEP-DOE 2).

there is a strong increase in variance in the eastern Pacific (241–300°E) during positive SAM compared to other longitudinal bands and to its opposite phase (Figures 4c,d).

4. Impact of SAM and ENSO on the Occurrence and Duration of LLRWPs

The time series of detected LLRWPs for a threshold of 19 m/s in ERA5 and the SAM index are correlated at -0.31 , significant at 5% level. On the other hand, the correlation between the same time series of LLRWPs and the ONI index is 0.19, which is not statistically significant at 10% level. Nevertheless, since the relationship between LLRWPs and ENSO may not be linear, in this section, we further explore the influence of SAM and ENSO on the distribution of the frequency of occurrence and duration of LLRWPs. Figure 5 shows the results for different thresholds and both reanalyses.

The tracking algorithm detected a larger number of LLRWPs during El Niño compared to neutral and La Niña years in NCEP-DOE 2 reanalysis. After applying the Kruskal Wallis test, we found that the differences in the occurrence of LLRWPs during El Niño and La Niña are statistically significant: the p-values obtained are 0.02 for low thresholds (13 m/s), 0.10 for medium thresholds (15 m/s), and 0.09 in high thresholds (17 m/s). Nonetheless, in the case of ERA5, these p-values are close but do not reach the minimum level of significance established, showing p-values of 0.12, 0.12, and 0.23 for low, medium, and high threshold. We also compared the duration of the trajectories during different ENSO phases and we did not find any significant differences. Thus, except for the low-threshold case in NCEP-DOE 2, differences between El Niño and La Niña are marginal or not significant suggesting that ENSO influence on LLRWPs is weak and not robust.

We next turn to the impact of SAM (Figure 6). In contrast to ENSO, independently of the threshold considered in ERA5, positive SAM events display the lowest frequency of occurrence of LLRWPs and negative SAM the highest, whereas neutral SAM shows intermediate values. Kruskal Wallis test results show that for ERA the occurrence of LLRWPs during positive SAM and negative SAM events are significantly different for all thresholds, showing p-values of 0.03, 0.02, and 0.03 for low, medium, and high thresholds, respectively. For the NCEP-DOE 2 data set, we only found statistically significant differences between positive and negative SAM for low threshold (p-values of 0.09, 0.5, and 0.20 for low, medium, and high thresholds). Results are also statistically significant between the interannual variability of positive SAM against neutral SAM for medium threshold (p-values of 0.21, 0.07, and 0.58 for low, medium, and high thresholds, respectively) in NCEP-DOE 2 data sets. (See also Table S1 in Supporting Information S1).

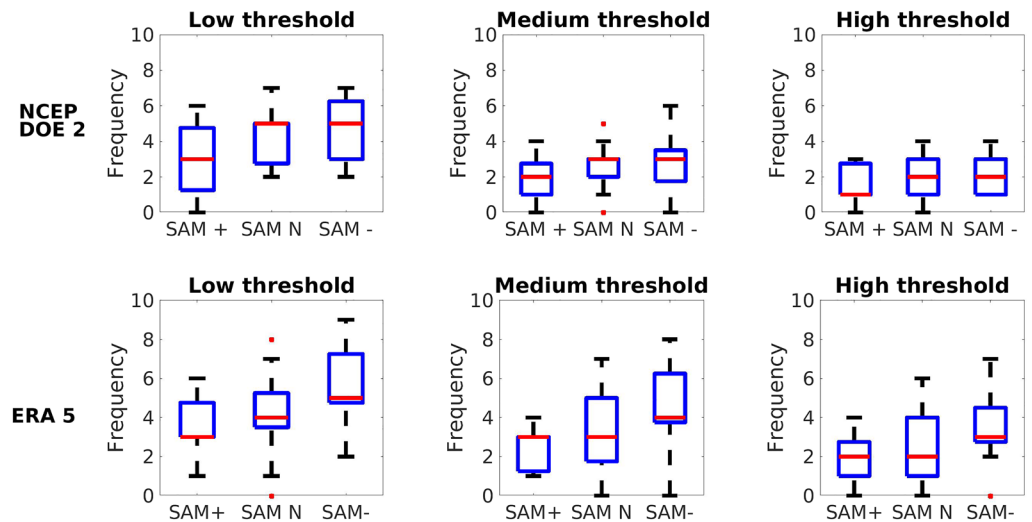


Figure 6. Analogous to Figure 5 but for SAM events.

In addition to increasing the frequency of occurrence, negative SAM events register LLRWPs that last longer compared to those detected during positive SAM years (Figure 7). The differences between the duration of LLRWPs during negative and positive SAM events are statistically significant at 10% level for low and medium thresholds in the ERA5 data set, (low, medium, and high thresholds show p-values of 0.03, 0.06, and 0.22), and for medium threshold in the NCEP-DOE 2, (p-values of 0.26, 0.09, and 0.44 for low, medium, and high thresholds). Moreover, the LLRWPs duration in positive SAM events is significantly smaller than that during neutral SAM events for low thresholds in ERA5 and for medium threshold in the case of NCEP-DOE 2 data set, (p-values of 0.06 and 0.09, respectively, see Table S1).

Overall, results obtained in this section suggest that SAM has a robust influence on the LLRWPs, such that negative SAM phases favor the occurrence of LLRWPs and that these packets last significantly longer compared to those detected during positive SAM phases. Conversely, ENSO impact is not robust as results depend on the reanalysis and threshold value used. El Niño seems to favor LLRWPs, but these results are not significant in the

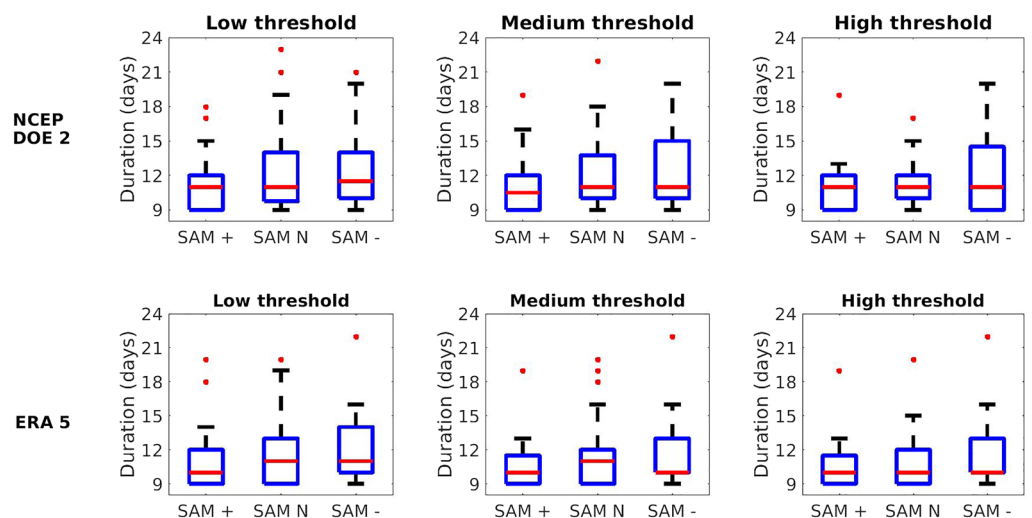


Figure 7. Boxplots of interannual LLRWPs duration for different SAM phases using NCEP-DOE 2 (upper panel) and ERA5 (lower panels) for different minimum thresholds. Red point crosses show the outliers and red lines show the median location. The title of each boxplot refers to the thresholds applied. Low threshold is 17 (13) m/s, medium threshold is 19 (15) m/s, and high threshold is 21 (17 m/s) for ERA5 (NCEP-DOE 2).

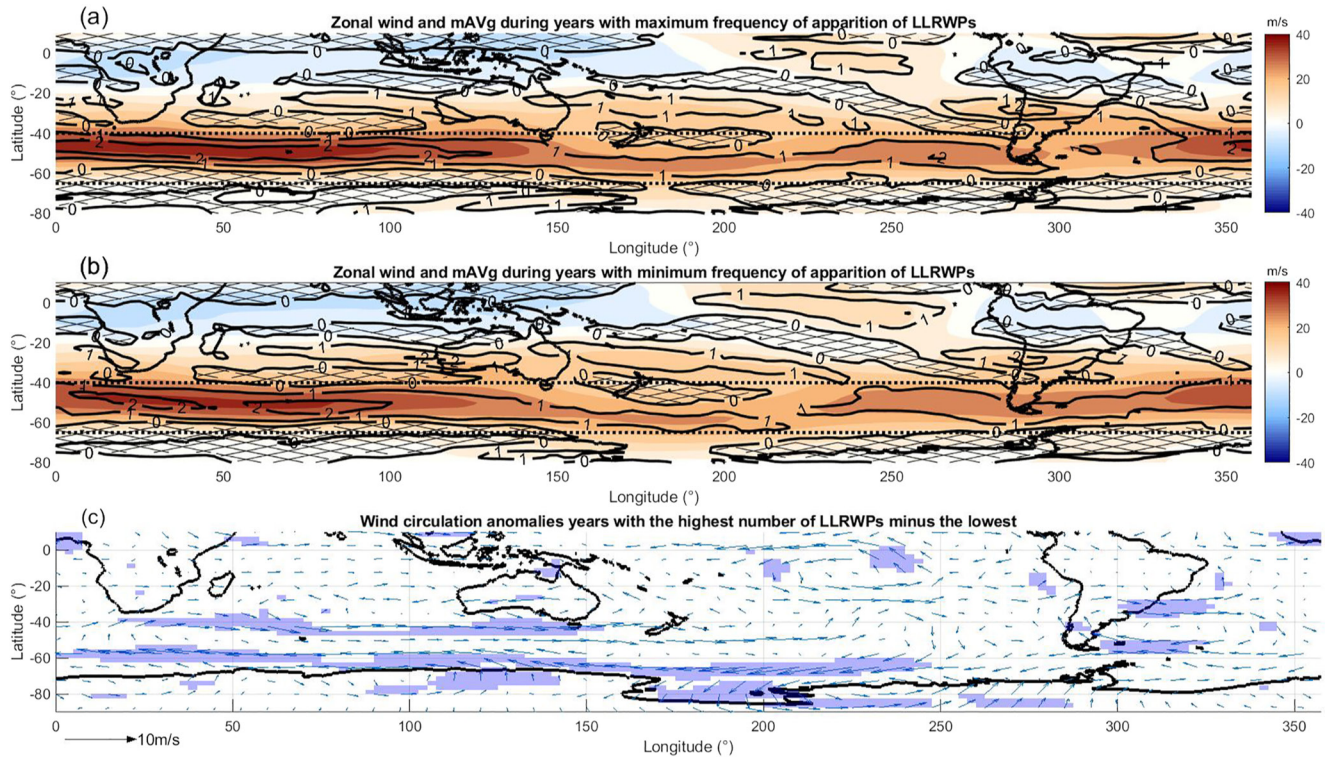


Figure 8. Composite maps of zonal wind speed (colored areas, expressed in m/s) and mAVg (lines, expressed in 10^{-10} /m/s), during years of maximum (a) and minimum (b) frequency of occurrence of LLRWPs in ERA5. Black lines show positive mAVg and areas with negative mAVg are highlighted with a hatching crossed pattern. Black dotted lines show the limits of the area of study. Panel c shows the wind circulation anomalies constructed as the difference between years of maximum and minimum LLRWPs. Blue areas indicate where the anomalies are statistically significant at 10% level.

ERA 5 reanalysis data. In the next section, we explore the mechanisms that favor LLRWPs and how SAM may modulate their occurrence

5. Conditions That Favor LLRWPs Propagation

Figure 8 displays the composite maps of u_{300} and mAVg during years with the highest (Figure 8a) and lowest (Figure 8b) LLRWPs frequency of occurrence. During the years of maximum frequency of occurrence of LLRWPs, the jet stream is stronger, more zonal, and narrower from the southeastern Atlantic until the southwestern Pacific. Both Figures 8a and 8b show a region with negative values of mAVg to the east of New Zealand. Since the mAVg must be positive to enable RWP propagation, in that region RWP propagation is either restricted or blocked (Hendon, 2018). This region of negative mAVg is larger, extending toward higher latitudes during years with the lowest frequency of occurrence of LLRWPs. To further understand the differences in mean wind conditions between years of maximum and minimum frequency of LLRWPs, Figure 8c shows the difference in the 300 hPa wind field. Consistent with the previous maps, circulation changes are characterized by westerly wind anomalies between 40 and 50°S in the Indian ocean sector and easterlies between 50 and 60°S over most of the domain. In addition, superposed on these zonal anomalies there are weak cyclonic circulation anomalies located in the southwestern Atlantic, southwest of Africa, and southwest of Australia.

To complement the above analysis, Figure 9a shows the regression fields of u_{300} , mAVg, Z_{300} , and SST anomalies onto the time series of the frequency of occurrence of LLRWPs. Consistent with Figure 8, the increase in LLRWPs is inversely correlated with an increase of zonal mean wind speed in the medium-high latitudes (50–65°S), whereas it is positively correlated with zonal wind speeds at lower latitudes (35–50°S). In the case of the mAVg (Figure 9b), we observe the same spatial pattern as for u_{300} , although the field is noisier. As during austral summer, the jet stream is approximately zonally symmetrical and centered in 50°S, results of Figures 8 and 9 suggest that northward (southward) displacement of the jet stream favors (disfavors) the propagation of LLRWPs.

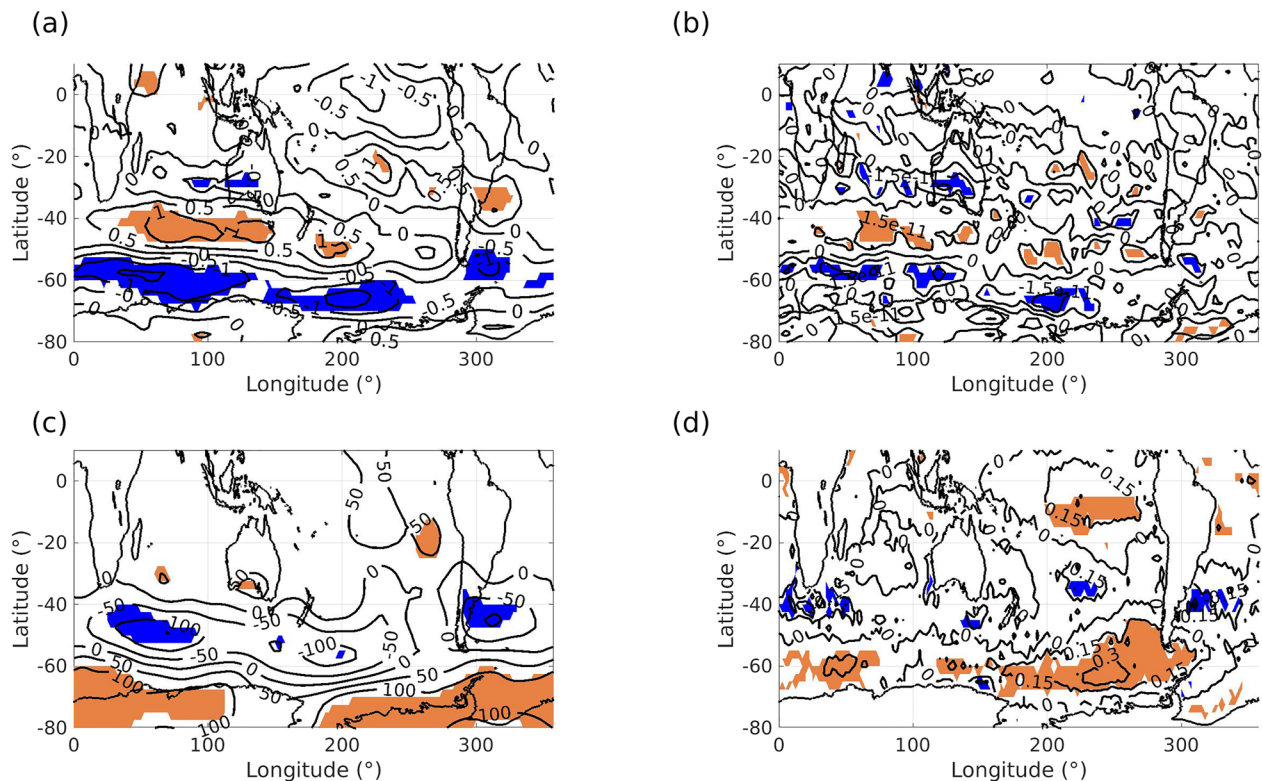


Figure 9. Linear regression-correlation maps of several fields onto the interannual frequency of occurrence of LLRWPs in ERA5: (a) zonal wind speed at 300 hPa (m/s), (b) mAVg (1/ms), (c) geopotential height at 300 hPa (m), and (d) SST anomalies ($^{\circ}\text{C}$). The colored areas indicate where the correlation is significant in the 10% level, with orange (blue) areas corresponding to positive (negative) values. Black lines display values of linear regression coefficient.

Accompanying these changes, there is a decrease in Z_{300} in midlatitudes and an increase in high latitudes, together with cyclonic circulations to the southwest of the continental areas as mentioned before (Figure 9c). Similar results are obtained using NCEP-DOE2 reanalysis (not shown). Thus, taken together these results suggest that years with a high number of LLRWPs are characterized by large-scale circulation anomalies that look very close to the negative phase of SAM (see also Figure S2). This is consistent with the results of Section 4, where negative SAM events were found to favor the occurrence and duration of LLRWPs. Figure 9d further shows that an increase in LLRWPs shows zonal bands of positive (negative) correlation with sea surface temperatures in high (mid) latitudes, consistent with atmospheric forcing. Lastly, a weak correlation with positive sea surface temperature anomalies in the tropical Pacific (Figure 9d) is also seen, again suggesting that El Niño may play a secondary role in setting large-scale conditions that favor LLRWPs propagation.

Why would a stronger, northward-shifted and narrow jet in the Indian-western Pacific basin favor LLRWPs? We hypothesize that this is because the climatological jet in the Atlantic-Indian sector acts as a better waveguide and extends further into the Pacific basin. To address this issue, we calculate the EOFs of the WCI between 30 and 70°S .

The leading EOF (EOF1) only explains 10% of the total variance, but the corresponding PC1 is highly correlated with the interannual variability of LLRWPs, showing a correlation of 0.51 (in ERA5, medium threshold), statistically significant at 5%. The second EOF is not related to the occurrence of LLRWPs and thus is not considered. Figure 10 shows the spatial pattern of the leading EOF, characterized by a dipolar structure with opposite values to the south and north of 50°S . The positive correlation indicates that an increase/decrease of the WCI in the midlatitudes is associated with an increase/decrease in the occurrence of LLRWPs. Additionally, the PC1 is negatively correlated with the SAM index (-0.46), and positively correlated with the ONI index (0.45), both results significant at 5%. The strong negative correlation with SAM indicates that during positive SAM, the WCI increases in high latitudes of the Indian-Pacific sector. Conversely, negative SAM phases are associated with an increase in WCI in midlatitudes from the Indian to the Pacific sector, indicating that the northward-shifted jet

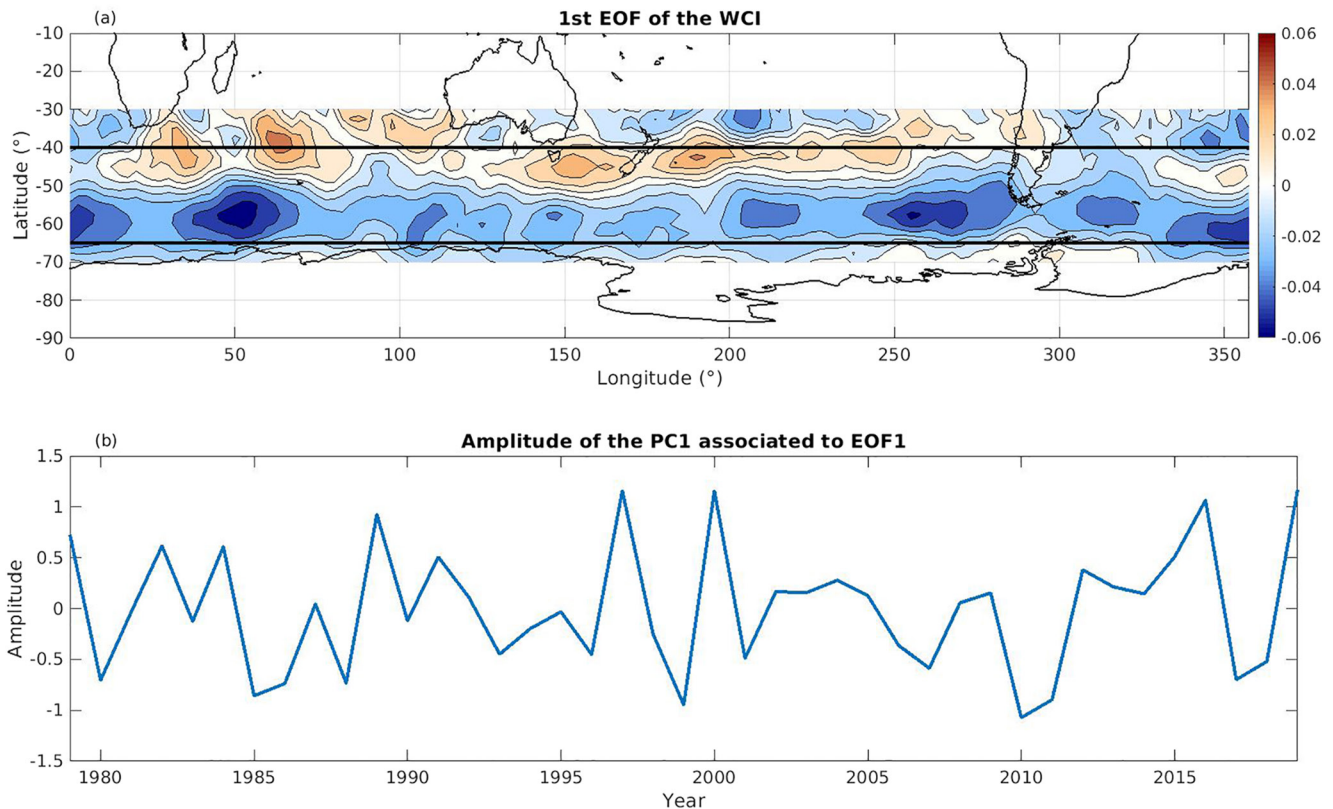


Figure 10. For ERA5, (a) leading EOF of the seasonal variability of the wave coherence index and (b) time series of the PC1.

is acting as a better waveguide compared to the southward-shifted jet during positive SAM phases, favoring the occurrence of LLRWPs.

The changes in the circulation associated with EOF1 are further explored in Figure 11. As expected from the correlation analysis, years with highest (lowest) amplitude of PC1 are characterized by large-scale circulation conditions similar to those during years of maximum (minimum) frequency of occurrence of LLRWPs (compare Figures 8a, 8b and 11a, 11b). Moreover, as in Figure 8c, the difference in wind circulation shows that years with maximum WCI in midlatitudes are characterized by a stronger, narrow and northward shifted jet in the Atlantic-Indian basin that extends into the Pacific sector (Figure 11c). The development of a cyclonic circulation anomaly to the southwest of Australia helps extending the jet into the Pacific. These are the conditions during the negative SAM phases. Conversely, during SAM-positive phases, the development of an anticyclonic circulation to the southwest of Australia blocks the jet and creates a region of negative meridional absolute vorticity gradient that prevents the propagation of wave packets, (see also Figure S2).

The signature of El Niño can also be distinguished in Figure 11c: weakened upper level equatorial westerlies, subtropical Pacific anticyclonic anomalies, and a strong anticyclonic center located about 110W, 70°S (e.g., Barreiro 2017). This explains the significant positive correlation of the PC1 with the ONI index. These circulation anomalies are also present, although weaker, in Figure 8c. It is important to note that ENSO teleconnections project onto SAM, such that El Niño tends to favor negative SAM phases (Gong et al., 2010). Thus, given that in Section 4 the ENSO signal is not found to be robust, it is likely that the relationship between ENSO and LLRWPs occurs indirectly through ENSO's connection with SAM.

6. Summary

A detection algorithm was implemented to study the interannual variability of RWPs, and in particular, the impact of SAM and ENSO on packets lasting longer than 8 days. We used ERA5 reanalysis as our main data set and compared the results obtained against NCEP-DOE 2 reanalysis data to test the robustness of the findings. Overall,

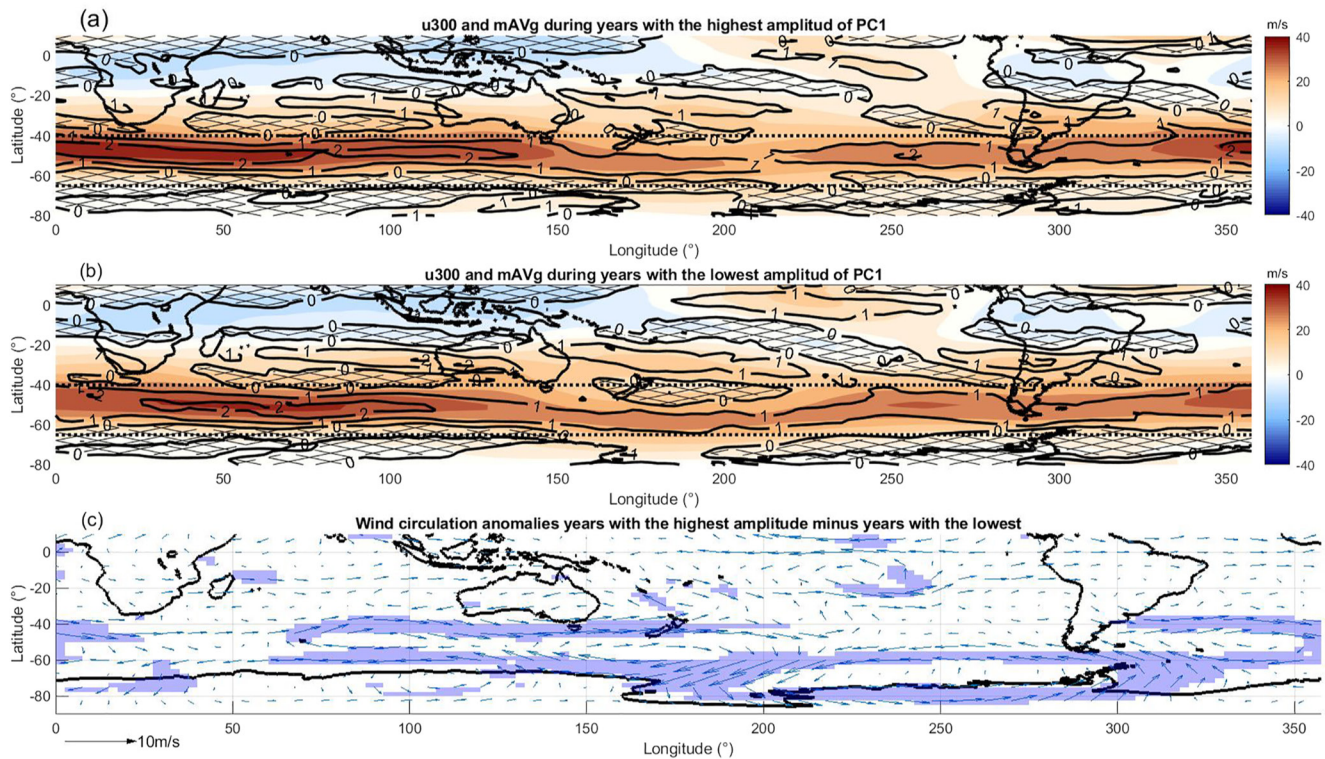


Figure 11. Analogous to Figure 8, but for the extremes of PC1.

we found more (less) LLRWPs that last longer (less) during negative (positive) phases of SAM in both reanalysis. Results show that during negative SAM phases, the jet shifts northward, strengthens in the Indian basin and extends further into the Pacific basin, so that it acts as a better waveguide favoring the propagation of LLRWPs. Conversely, during positive phases of SAM, the jet shifts southward and an anticyclonic center develops to the southwest of Australia blocking the jet and the progression of the wave packets. It is worth pointing out that years with neutral SAM conditions tend to show intermediate numbers of LLRWPs.

The impact of ENSO on LLRWPs is not robust. We suggest that the weak relationship found may be due to the effect of ENSO on SAM. Gong et al. (2010) suggested that El Niño may set background conditions that favor negative SAM events and La Niña does similarly for positive SAM events. Thus, this may result in an indirect correlation between ENSO and the occurrence of LLRWPs.

Thus, the results found in this study suggest that LLRWPs are more common during years with negative SAM phases. Given their link with extreme weather events, our findings are indicative that extended range forecasting of extreme events may be more feasible during negative SAM years and will be less skillful when La Niña and positive SAM phases are present.

Data Availability Statement

ERA5 reanalysis data are freely available in the Copernicus Climate Data Store <https://cds.climate.copernicus.eu/>. NCEP/DOE Reanalysis 2 can be downloaded at the websites: https://psl.noaa.gov/data/gridded/data.ncep_reanalysis2.html. ENSO and SAM indexes are available at <https://origin.cpc.ncep.noaa.gov/>. The amplitude of the envelope of the RWPs is publicly available at <https://doi.org/10.5281/zenodo.5714192>, as well as a script to obtain wind envelope data from meridional wind speed at <https://doi.org/10.5281/zenodo.5724656>.

Acknowledgments

This project has received funding from the European Union's Horizon 2020 research and innovation programme under the Marie Skłodowska-Curie grant agreement No 813844 (ITN CAFÉ). C.M acknowledges partial support from Spanish Ministerio de Ciencia, Innovación y Universidades (PGC2018-099442-B-I00) and from ICREA ACADEMIA program of Generalitat de Catalunya.

References

Barreiro, M. (2017). Interannual variability of extratropical transient wave activity and its influence on rainfall over Uruguay. *International Journal of Meteorology*, 37, 4261–4274. <https://doi.org/10.1002/joc.5082>

Barreiro, M., Diaz, N., & Renom, M. (2014). Role of the global oceans and land-atmosphere interaction on summertime interdecadal variability over northern Argentina. *Climate Dynamics*, 42, 1733–1753. <https://doi.org/10.1007/s00382-014-2088-6>

Branstator, G. (2002). Circulmglobal Teleconnections, the jet stream waveguide, and the North Atlantic oscillation. *Journal of Climate*, 15(14), 1893–1910. [https://doi.org/10.1175/1520-0442\(2002\)015<1893:CTTJSW>2.0.CO;2](https://doi.org/10.1175/1520-0442(2002)015<1893:CTTJSW>2.0.CO;2)

Chang, E. K. M. (1999). Characteristics of wave packets in the upper troposphere. Part II: Seasonal and hemispheric variations. *Jornal of Atmospheric Sciences*, 56(11), 1729–1747. [https://doi.org/10.1175/1520-0469\(1999\)056<1729:COWPIT>2.0.CO;2](https://doi.org/10.1175/1520-0469(1999)056<1729:COWPIT>2.0.CO;2)

Chang, E. K. M. (2000). Wave Packets and Life Cycles of Troughs in the Upper Troposphere: Examples from the Southern Hemisphere, Summer Season of 1984/1985. *Monthly Weather Review*, 128(1), 25–50. [https://doi.org/10.1175/1520-0493\(2000\)128<0025:WPALCO>2.0.CO;2](https://doi.org/10.1175/1520-0493(2000)128<0025:WPALCO>2.0.CO;2)

Chang, E. K. M. (2005). The Impact of Wave Packets Propagating across Asia on Pacific Cyclone Development. *Monthly Weather Review*, 133(7), 1998–2015. <https://doi.org/10.1175/MWR2953.1>

Chang, E. K. M., & Yu, D. B. (1999). Characteristics of wave packets in the upper troposphere. Part I: Northern Hemisphere winter. *Jornal of Atmospheric Sciences*, 56(11), 1708–1728. [https://doi.org/10.1175/1520-0469\(1999\)056<1708:cowpit>2.0.co;2](https://doi.org/10.1175/1520-0469(1999)056<1708:cowpit>2.0.co;2)

Gong, T., Feldestein, B. S., & Luo, D. (2010). The Impact of ENSO on Wave Breaking and Southern Annular Mode Events. *Journal of the atmospheric Sciences*, 67, 2854–2870. <https://doi.org/10.1175/2010JAS3311.1>

Grazzini, F., & Lucarini, V. (2010). *Climatology of extratropical atmospheric wave packets in the Northern Hemisphere*. <https://arxiv.org/abs/1011.3564>

Grazzini, F., & Vitart, F. (2015). Atmospheric predictability and Rossby wave packets. *International Journal. of the Royal . Meteorological. Society*, 141(692), 2793–2802. <https://doi.org/10.1002/qj.2564>

Hans, H., Bell, B., Berrisford, P., Hirahara, S., Horány, A., Muñoz-Sabater, J., & Nicolas, J. (2020). The ERA5 global reanalysis. *Royal Meteorological Society*, 146(730), 1999–2049. <https://doi.org/10.1002/qj.3803>

Hendon, H., & Hendon, H. H. (2018). Understanding Rossby wave trains forced by the Indian Ocean dipole. *Climate Dynamics*, 50(50), 2783–2798. <https://doi.org/10.1007/s00382-017-3771-1>

Hoskins, B. J., & Ambrizzi, T. (1993). Rossby Wave Propagation on a realistic Longitudinally Varying Flow. *Journal of Atmospheric Science*, 50(12), 1661–1671. [https://doi.org/10.1175/1520-0469\(1993\)050<1661:RWPOAR>2.0.CO;2](https://doi.org/10.1175/1520-0469(1993)050<1661:RWPOAR>2.0.CO;2)

Kanamitsu, M., Ebuzuzaki, W., Woollen, J., Yang, S.-K., Hnilo, J. J., Fiorino, M., & Potter, L. G. (2002). NCEP-DOE AMIP- II Reanalysis R-2. *American Meteorology Society*, (Vol. 83, pp. 1631–1644). <https://doi.org/10.1175/BAMS-83-11-1631>

Manola, I., Selten, F., H de Vries, H., & Hazeleger, W. (2013). "Wavguidability" of idealized jets. *Journal of Geophysical Research-Atmospheres*, 118(18), 10432–10. <https://doi.org/10.1002/jgrd.50758>

O'Brien, L., & Reeder, J. M. (2017). Southern Hemisphere Summertime Rossby Waves and Weatherin the Australian Region. *Quarterly Journal of the Royal Meteorologica Society*, 143(707), 2374–2388. <https://doi.org/10.1002/qj.3090>

Sagarra, R., & Barreiro, M. (2020). Characterization of extratropical waves during summer of the Southern Hemisphere. *Meteorologica*, 45, 63–79.

Seager, R., Henderson, N., Ting, M., Cane, A. M., Harnik, N., & Kushnir, Y. (2010). Adjustment of the atmospheric circulation to tropical Pacific SST anomalies: Variability of transient eddy propagation in the Pacific- North America sector. *Quarterly Journal of the Royal Meteorological Society*, 136, 277–296. <https://doi.org/10.1002/qj.588>

Souders, B. M., Colle, A. B., & Chang, M. K. D. (2014a). The climatology and characteristics of Rossby Wave Packets using a feature-based tracking technique. *Monthly Weather Review*, 142(10), 3528–3548. <https://doi.org/10.1175/MWR-D-13-00371.1>

Souders, B. M., Colle, A. B., & Chang, M. K. D. (2014b). A Description and Evaluation of an Automated Approach for Feature-Based Tracking of Rossby Wave Packets. *Monthly Weather Review*, 142(10), 3505–3527. <https://doi.org/10.1175/MWR-D-13-00317.1>

Teng, H., & Branstator, G. (2019). Amplification of Waveguide Teleconnections in the Boreal Summer. *Mid-latitude Processes and Climate Change*, 5, 421–432. <https://doi.org/10.1007/s40641-019-00150-x>

Trenberth, E. K. (1981). Observed Southern Hemisphere Eddy Statistics at 500 mb: Frequency and Spatial Dependence. *Journal of Atmospheric Science*, 38(12), 2585–2605. [https://doi.org/10.1175/1520-0469\(1981\)038<2585:OSHESA>2.0.CO;2](https://doi.org/10.1175/1520-0469(1981)038<2585:OSHESA>2.0.CO;2)

Yeh, T. C. (1949). On energy dispersion in the atmosphere. *Journal of Meteorology*, 6(1), 1–16. [https://doi.org/10.1175/1520-0469\(1949\)006<0001:OEDITA>2.0.CO;2](https://doi.org/10.1175/1520-0469(1949)006<0001:OEDITA>2.0.CO;2)

Wirth, V. (2020). Wavguidability of idealized midlatitude jets and the limitations of ray tracing theory. *Weather Climate Dynamics*, 1, 111–125. <https://doi.org/10.5194/wcd-1-111-2020>

Wirth, V., Riemer, M., Chang, E. K. M., & Martius, O. (2018). Rossby Wave Packets on the Midlatitude waveguide- a review. *Monthly Weather Review*, 146(7), 1965–2001. <https://doi.org/10.1175/MWR-D-16-0483.1>

Xu, P., Wang, L., & Chen, W. (2019). The British-Baikal Corridor: A teleconnection pattern along the summertime polar front jet over Eurasia. *Journal of Climate*, 32(3), 877–896. <https://doi.org/10.1175/JCLI-D-18-0343.1>

Xu, P., Wang, L., Vallis, K. G., Geen, R., Screen, J. A., Wu, P., & Ding, S. (2021). Amplified Waveguide Teleconnections Along the Polar Front Jet Favor Summer Temperature Extremes Over Northern Eurasia. *Geophysical Research Letters*, 48(13). <https://doi.org/10.1029/2021GL093735>

Zheng, M., Chang, E. K., & Colle, B. A. (2013). Ensemble sensitivity tools for assessing extratropical cyclone intensity and track predictability. *Weather and Forecasting*, 28(5), 1133–1156. <https://doi.org/10.1175/WAF-D-12-00132.1>

Zimin, A. V., Szunyogh, I., Hunt, R. B., & Ott, E. (2006). Extracting envelopes of Nonzonally Propagating Rossby Wave Packets. *Monthly Weather Review*, 134(4), 1329–1333. <https://doi.org/10.1175/MWR3122.1>

Zimin, V. A., Szunyogh, I., Patil, J. D., Hunt, R. B., & Ott, E. (2003). Extracting envelopes of Rossby Wave Packets. *Monthly Weather Review*, 131(5), 1011–1017. [https://doi.org/10.1175/1520-0493\(2003\)131<1011:EEORWP>2.0.CO;2](https://doi.org/10.1175/1520-0493(2003)131<1011:EEORWP>2.0.CO;2)